5 March 2002

ELSEVIER

Chemical Physics Letters 354 (2002) 120–127

CHEMICAL PHYSICS LETTERS

www.elsevier.com/locate/cplett

The photodissociation of $ClNO_2$ in argon and water clusters studied at 235 nm by the REMPI-TOF method

Qiang Li, J. Robert Huber *

Physikalisch-Chemisches Institut der Universität Zürich, Winterthurerstrasse 190, CH-8507 Zürich, Switzerland

Abstract

The photodissociation of $ClNO_2$ embedded in argon and water clusters was investigated at 235 nm by detecting the $Cl(^2P_{3/2})$ photofragments with resonance enhanced multiphoton ionization time-of-flight spectroscopy (REMPI-TOF). Under various cluster formation conditions the speed distributions of $Cl(^2P_{3/2})$ were recorded. In contrast to the monomer photolysis only one decay channel was found to be active showing the fragments to be Boltzmann distributed and isotropic. In view of atmospheric chemistry, $ClNO_2$ in water clusters is a photolytical source of Cl and NO_2 radicals with low translational and internal energy. They are thus less favorable for consecutive reactions than the monomer products.

1. Introduction

Nitryl chloride, $ClNO_2$, is a molecule of atmospheric interest. It is formed by heterogeneous reactions of gaseous N_2O_5 with HCl on ice surfaces in the stratospheric clouds and by N_2O_5(g) with NaCl(s) in the marine boundary layer [1–3]. Both of these reactions are significant in atmospheric chemistry because they convert inert solid chloride to a gas phase active chlorine compound. Recently, the emission inventories for major reactive chlorine species have been explored and based on a general circulation model the concentration of $ClNO_2$ has been calculated [4,5]. Behnke et al. [6], studying the interactions between N_2O_5 and NaCl in an aerosol smog chamber, proposed a formation mechanism for $ClNO_2$. Exposed to solar radiation this product is readily photolysed to provide Cl and NO_2 [7–9]. It has therefore been suggested that $ClNO_2$ plays a role in photochemical air pollution in the marine troposphere [1,10] and in catalytic ozone depletion in the stratosphere [2,3,11,12].

The UV spectrum of $ClNO_2$ at room temperature starts with a weak, unstructured absorption between 300 and 400 nm followed by an onset at around 280 nm, a peak at 215 nm ($\sigma = 3.2 \times 10^{-18}$ cm^2) and a strong increase below 200 nm [7,8,13]. For the present study we used an excitation wavelength of 235 nm ($\sigma = 1.5 \times 10^{-18}$ cm^2 [13]) which corresponds to 508 kJ/mol. Under these conditions the following reaction channels are energetically accessible according to thermochemical data [14].

$$ClNO_2 + h\nu \rightarrow Cl + NO_2 \quad \Delta H = 138\ \text{kJ/mol} \tag{1}$$

$$\rightarrow ClO + NO \quad \Delta H = 174\ \text{kJ/mol} \tag{2}$$

* Corresponding author. Fax: +41-1-6356838.
E-mail address: jrhuber@pci.unizh.ch (J. Robert Huber).

0009-2614/02/$ - see front matter
PII: S0009-2614(02)00120-3

$$\rightarrow \mathrm{ClNO} + \mathrm{O} \quad \Delta H = 283\,\mathrm{kJ/mol} \quad (3)$$

$$\rightarrow \mathrm{Cl} + \mathrm{O} + \mathrm{NO} \quad \Delta H = 439\,\mathrm{kJ/mol} \quad (4)$$

The reaction enthalpies refer to the products in their electronic ground states. However, it is possible that the photofragments are formed in electronically excited states which is relevant for the Cl and O atoms having low lying spin-orbit excited states and also for the NO_2 molecule where the A^2B_2, B^2B_1 and C^2A_2 states lie at 9726, 14 743 and 16 360 cm^{-1} above the X^2A_1 ground state, respectively [15–17].

To the best of our knowledge, there is no evidence for the rearrangement of the molecule leading to ClO + NO (channel 2) and for the three-body decay process to Cl + O + NO (channel 4) [13]. The photodissociation of $ClNO_2$ at 350 nm has been studied earlier by Johnston and coworkers using resonance fluorescence detection of Cl and O atoms [8]. Dissociation of the N–Cl bond to yield Cl + NO_2 (channel 1) was found to be the dominant process with a quantum yield of $\phi(\mathrm{Cl}) = 0.93 \pm 0.15$; the decay path to ClNO + O (channel 3) was of minor importance ($\phi(\mathrm{O}) < 0.02$). In addition, after excitation at 308 and 235 nm they observed a broad emission from electronically excited NO_2 fragments, but could not identify the emitting states [18]. Recently Carter et al. [19] investigated the 235 nm photodissociation of $ClNO_2$ by the REMPI-TOF detection method. A bimodal velocity distribution of the nascent Cl atoms in the $^2P_{3/2}$ ground state was observed which led to the conclusion that two decay channels are active in reaction (1):

$$\mathrm{ClNO_2} + h\nu \rightarrow \mathrm{Cl} + \mathrm{NO_2}(\mathrm{X^2A_1}) \quad (1a)$$

$$\rightarrow \mathrm{Cl} + \mathrm{NO_2}(\mathrm{A^2B_2}) \quad (1b)$$

The minor reaction leads to $NO_2(X^2A_1)$ with $\phi = 0.15 \pm 0.05$, the dominant one to $NO_2(A^2B_2)$ with $\phi = 0.85 \pm 0.05$. Using photofragment translation energy spectroscopy (PTS) [13] at 248 nm this study was extended confirming the formation of NO_2 fragments in the first electronically excited state A^2B_2. Furthermore the internal energy distribution of the NO_2 fragments obtained from the well-structured translational energy distribution revealed the NO_2 fragments to be produced not only in the electronic ground state X^2A_1 ($\sim 30\%$) and the excited electronic states A^2B_2 ($\sim 30\%$), but probably also in the B^2B_1 state ($\sim 40\%$).

Very recently, Plenge et al. [20] reported results on the photofragmentation of $ClNO_2$ at 240 and 308 nm employing photoionization mass spectrometry. For the two important channels (1) and (3) they found $\phi(\mathrm{Cl}) = 0.93 \pm 0.10$ and $\phi(\mathrm{O}) = 0.07 \pm 0.01$, respectively after 308 nm excitation. However, at 240 nm the Cl production was found to be significantly reduced relative to that of oxygen ($\phi(\mathrm{Cl})/\phi(\mathrm{O}) = 1.44 \pm 0.15$) which could not be conciliated with previous results. At both photolysis wavelengths the atomic oxygen was formed in its $^3P_2$ ground state.

Owing to the potential importance of the photodissociation of nitric acid, $HONO_2$, attached to ice particles in the stratosphere [21–23] we studied water-clustered $HONO_2$ at 193 nm [24]. This photolysis wavelength reproduces well the solar photolysis conditions in the stratosphere, where the 190–230 nm region is largely unfiltered by O_3, O_2 and N_2. In the same spirit we explored $ClNO_2$ (an isovalent molecule of $HONO_2$) and report here the results of the 235 nm photodissociation of $ClNO_2$ attached to or embedded in Ar and H_2O clusters with an average cluster size $n \sim 200$–800. Using resonance enhanced multiphoton ionization time-of-flight spectroscopy (REMPI-TOF) the velocity distribution of the $Cl(^2P_{3/2})$ fragments emerging from clustered $ClNO_2$ was investigated and compared to results previously obtained from $ClNO_2$ monomer photolysis.

2. Experiment

The apparatus has been described in some detail elsewhere [25,26]. Briefly, it consists of a molecular beam source chamber, pumped by two diffusion pumps, and a main chamber, separated by a skimmer and equipped with a time of flight mass spectrometer (TOF-MS). The main chamber is pumped by two turbomolecular pumps, one mounted directly below the MS accelerator stage and one at the detector end of the flight tube. The

TOF-MS is a two stage Wiley–McLaren design with an extraction and an acceleration region [27]. Two orthogonal pairs of deflection plates allow any drift in the ion trajectories to be corrected. The photofragment ions are detected by a multichannel plate detector (Galilleo FT 4000) which is mounted at the end of a 40 cm long field-free flight tube. The ion signal is amplified by a 500 MHz preamplifier and digitized by a 500 MHz digital sampling oscilloscope (HP5422A). A sufficient signal to noise ratio for the TOF measurements is typically achieved after about 500 shots.

The photodissociation experiments were carried out with a Lambda Physik FL2002 dye laser pumped by a Lambda Physik LPX200 excimer laser running on XeCl at 308 nm. The laser beam is focused by a 40 cm focal length lens into the middle of the extraction region of the TOF-MS where it crosses the molecular beam. In the present work, the dye laser pulse ran on Coumarin 47 and the output was frequency doubled with a BBO crystal yielding a pulse energy of 400 μJ around 235 nm with a bandwith of 0.4 cm^{-1}. Measurements on the Cl photofragments were performed using a one-colour arrangement in which the same dissociation laser pulse was used for both dissociation and detection. The $Cl^2\ P_{3/2}$ atomic ground state was probed by $(2+1)$ REMPI at 235.27 nm via the $4p\ ^2D^o_{3/2} \leftarrow 3p^5\ ^2P^o_{3/2}$ transition [28]. The dissociation laser was linearly polarized to ~97% and the polarization could be rotated by a suitable $\lambda/2$ plate. The photodissociation experiments were carried out with parallel ($\chi = 0°$), perpendicular ($\chi = 90°$), and magic angle ($\chi = 54.7°$) polarizations relative to the detection axis. The photofragment speed distributions $P(v)$ were obtained from the TOF data using a forward convolution procedure as previously described [26].

Nitryl chloride was synthesized by passing HCl gas through a mixture of nitric and sulfuric acid and collecting the product in a low-temperature bath [29]. In order to generate the cluster beam, a conical nozzle (aperture $d = 1$ mm, length 10 mm, opening angle $2\theta = 20°$) mounted on a piezoelectric pulsed valve was used. Ar cluster with $ClNO_2$ was generated by expanding a premixture of 0.5–2% $ClNO_2$ in Ar at a backing pressure of 2 bar Ar. In the case of water cluster formation, a mixture of 0.4% $ClNO_2$ in 2 bar He was guided into a flask filled with H_2O at temperature between 30 and 65 °C. The outgoing gas mixture, possessing a partial pressure of $p(H_2O) = 40$–250 mbar, was then passed through a heated tube to the pulsed valve. The latter was also heated to prevent condensation of water. Based on the work of Buck and Krohne [30] and Hagena [31], the average cluster size for the argon and the water clusters is expected to be in the range of ~200–400 and ~400–800, respectively.

3. Results

The TOF profiles recorded for the $Cl(^2P_{3/2})$ fragments following photodissociation of Ar_nClNO_2 and $(H_2O)_nClNO_2$ clusters at 235.27 nm are displayed in Fig. 1a and b for the laser polarization parallel, at the magic angle and perpendicular to the detection axis, respectively. The feature on the right-hand side of the profiles is due to the onset of the corresponding TOF profile of the ^{37}Cl isotope. The analysis by a forward convolution procedure [26] yielded three speed distributions $P(v)$ of Cl photofragments indicated as dotted, dashed and chain-dashed lines. These distributions are shown in Fig. 2a and b for the Ar_nClNO_2 and $(H_2O)_nClNO_2$ clusters, respectively. The main, middle component (dashed line) consists of ~62% and 60% of all the detected Cl fragments from the Ar_nClNO_2 and the $(H_2O)_n$ $ClNO_2$ clusters, respectively, and is centered at ~1600 m/s for both distributions. The faster component (chain-dashed lines) consists of 14% and 12% of the detected Cl fragments from Ar_nClNO_2 and $(H_2O)_nClNO_2$, respectively, and has a mean speed of ~2700 m/s for both clusters. The analysis further revealed that the two components have the same anisotropy parameter $\beta = +1.0 \pm 0.1$ in both types of cluster dissociations. The ratio between the two components is thus about 82:18. Based on the earlier findings of the monomer photodissociation performed at the same excitation wavelength [19], we assign the fast component of the Cl fragment distributions to reaction (1a) with the products $Cl + NO_2\ (X^2A_1)$ and the middle component to

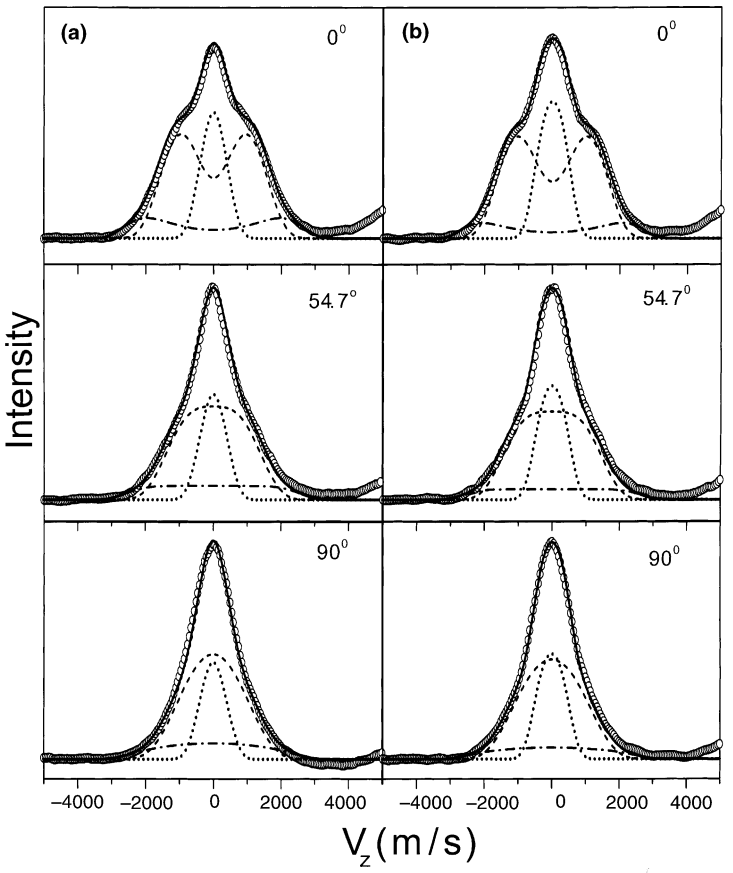

Fig. 1. REMPI-TOF spectra of $Cl(^2P_{3/2})$ fragments from $ClNO_2$ photodissociation at 235 nm recorded under three different polarization angles for (a) argon clusters and (b) water clusters. The expansion conditions were: (a) 2 bar Ar with 0.5% $ClNO_2$, (b) 2 bar He with 0.4% $ClNO_2$ and 250 mbar H_2O. The open circles are the experimental data. The dotted line indicates Cl fragments from cluster dissociation, the chain-dashed line those from channel 1(a), and the dashed line those from channel 1(b); the soild line is the sum of the three contributions. The corresponding photofragment speed distributions are given in Fig. 2.

reaction (1b) with the products $Cl + NO_2(A^2B_2)$. For the monomer we previously found the two Cl speed distributions centered at 2700 and 1700 m/s and the ratio between the slow and fast component 85:15 [19]. Thus, all these data are the same for monomer and cluster photolysis within experimental error. On the other hand, the slow component (indicated by dotted lines in Fig. 2), which accounts for 24% and 28% of all detected Cl fragments, has a mean speed of 590 and 620 m/s for Ar_nClNO_2 and $(H_2O)_nClNO_2$ clusters, respectively. Both cluster types show the fragment anisotropy parameter to be $\beta = 0.0 \pm 0.1$. This component of the Cl products is attributed to emerge from the photodissociation of $ClNO_2$ incorporated in clusters (see below).

In order to explore cluster formation and cluster size distribution, the $ClNO_2$ concentration in the premixed samples with Ar and H_2O was varied. Fig. 3 shows the effect on the TOF profiles of the Cl photofragments on reducing the $ClNO_2$ concentration in Ar from 2% to 0.5% while keeping the Ar stagnation pressure at 1.5 bar. A distinct, relative increase of a factor of almost two (from 11% to 20%) is observed for the slow component in Fig. 3a paralleled by a corresponding increase of the isotropic part shown in Fig. 3b (center portion). Moreover the distribution of the

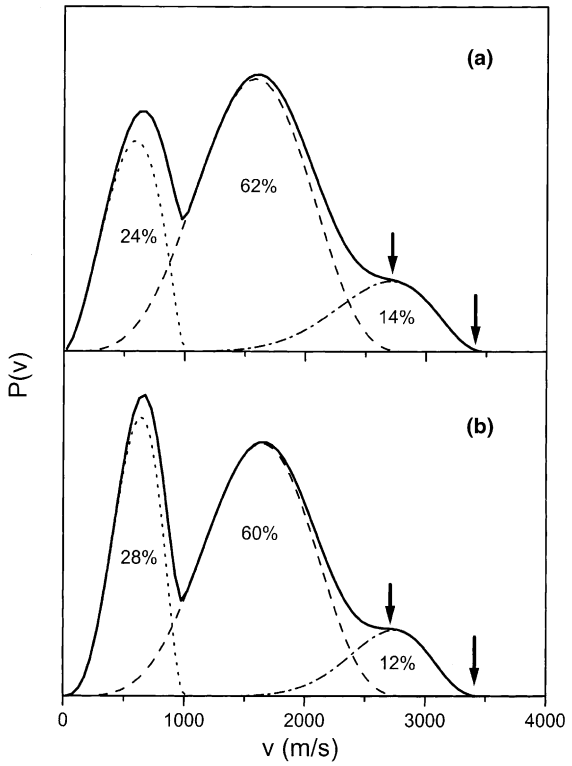

Fig. 2. $Cl(^2P_{3/2})$ photofragment speed distributions $P(v)$ from the REMPI-TOF data in Fig. 1, (a) Ar_nClNO_2 and (b) $(H_2O)_nClNO_2$. The dotted, dashed and chain-dashed lines indicate Cl fragments form cluster dissociation, from channel 1(b) and from channel 1(a), respectively. The arrows mark the maximum thermodynamically allowed speed E_T^{max} for the respective component.

slow Cl fragments is narrowed and its mean velocity shifted from 750 to 590 m/s due to this decrease in the $ClNO_2$ concentration. A similar effect is observed when the stagnation pressure of Ar is increased. Going from 1.5 to 2.5 bar and keeping the $ClNO_2$ concentration constant at 0.5%, the relative increase of the slow component is from 20% to 31% accompanied by a narrowing of its distribution. In both cases, i.e. for the $ClNO_2$ concentration decrease and the Ar pressure increase, the velocity distributions of the fast and medium components of the Cl fragments remain unchanged.

The corresponding results for the $(H_2O)_nClNO_2$ clusters are displayed in Fig. 4. It shows the speed distributions for $Cl(^2P_{3/2})$ photofragment stemming from photodissociation in an expansion of 0.4% $ClNO_2$ in 2 bar He with varying H_2O partial pressures. The fraction of the slow component is observed to increase with the water partial pressure from 9% at $p(H_2O) = 40$ mbar to 28% at 250 mbar. This is accompanied by a decrease in the mean speed of the slow component which falls from 700 to 620 m/s and by a decrease of the distribution width. The mean speed of the middle and fast component depends only slightly on (pH_2O) as evident from the reduction from 1750 and 2800 m/s at $p(H_2O) = 40$ mbar H_2O to 1650 and 2700 m/s at $p(H_2O) = 250$ mbar H_2O, respectively.

The cluster formation of $(H_2O)_nClNO_2$ and Ar_nClNO_2 was recorded by the $Cl(^2P_{3/2})$ signal as a function of the stagnation pressure. The $(H_2O)_nClNO_2$ cluster measurements were carried out using a mixture of 0.4% $ClNO_2$ in He at a pressure of 0.4 to 2.5 bar and a constant H_2O partial pressure of 200 mbar. The signal intensity for the slow component, which exclusively reflects cluster formation, is depicted in Fig. 5. It shows an abrupt increase at ~0.9 bar reaching a constant maximum value at ~1.4 bar. This behavior is reminiscent of a "phase transition" associated with cluster formation [25,26]. At a stagnation pressure below the onset pressure, the TOF profile is bimodal paralleling that of the monomer dissociation while pressures above the threshold yield trimodal profiles which contain the additional slow component. A similar behavior was observed for Ar_nClNO_2 as obtained with a mixture of 0.1% $ClNO_2$ in Ar and a changing pressure from 0.4 to 2.5 bar. The phase transition occurs here between ~0.8 and 1.2 bar (cf. Fig. 5).

4. Discussion

The photodissociation of $ClNO_2$ monomer at 235 nm has been studied by the REMPI-TOF method detecting the Cl ground state $(^2P_{3/2})$ photofragment [19]. Two contributions were observed in the speed distribution of $Cl(^2P_{3/2})$, $15 \pm 5\%$ of the fragments centered at 2700 m/s and $85 \pm 5\%$ centered at 1700 m/s. The fast fragments

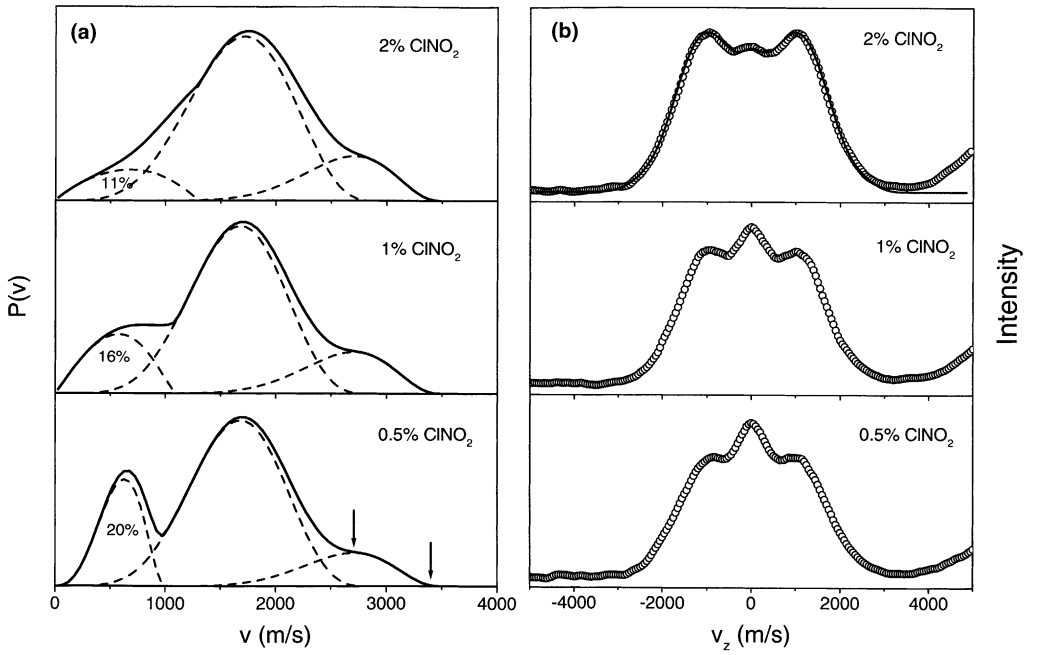

Fig. 3. REMPI-TOF spectra of $Cl(^2P_{3/2})$ photofragments (b) and the corresponding speed distributions $P(v)$ (a), as a function of the $ClNO_2$ concentration seeded in Ar at a stagnation pressure of 1.5 bar. The arrows mark E_T^{max}.

were attributed to decay channel 1(a) and the slow ones to 1(b) where the NO_2 counterfragment emerges in the ground X^2A_1 and electronically excited A^2B_2 state, respectively. The recoil anisotropy β was measured to be $+1.1 \pm 0.1$, suggesting a transition dipole moment along the N–Cl bond to an excited electronic state of A_1 symmetry. The dissociation lifetime estimated from this β value is shorter than 2.2 ps. At the excitation wavelength of 235 nm corresponding to 508 kJ/mol, the available energy E_{avl} obtained by the energy balance

$$E_{avl} = h\nu - D_o(Cl - NO_2) + E_{int}(ClNO_2), \qquad (1c)$$

is 370 kJ/mol; the dissociation energy D_o (Cl–NO_2) is 138 kJ/mol [14] and the internal energy of the parent molecule $E_{int}(ClNO_2)$ in the supersonic jet can be neglected. As the average total translational energy $\langle E_T \rangle$ was measured to be ~220 kJ/mol for channel (1a) and ~100 kJ/mol for channel (1b) [19], the internal energy $E_{vib} + E_{rot}$ is thus 150 kJ/mol for $NO_2(X^2A_1)$ and 154 kJ/mol for $NO_2(A^2B_2)$. The electronic excitation of the latter amounts to 116 kJ/mol [15].

The Cl photofragement speed distribution recorded under various cluster formation conditions are shown in Fig. 3 for Ar_nClNO_2, and in Fig. 4 for $(H_2O)_nClNO_2$ illustrating the influence of a cluster environment on the photofragmentation of $ClNO_2$. While for the monomer dissociation a bimodal speed distribution of the Cl fragment has been found [19], we observed three speed distributions. The analysis revealed that the fast and the medium component, which show the same intensity ratio and the same speed maxima under the various conditions applied, parallel the behavior of the two components found in the monomer dissociation for reactions (1a) and (1b). Furthermore the recoil anisotropy for both of these components, their non-Boltzmann speed distributions and the absence of a phase transition with increasing stagnation pressure are in excellent agreement with the monomer photolysis [19]. Thus only the slow speed component in Figs. 3 and 4 appears to be due to the $ClNO_2$ fragmentation in the cluster environment, while the majority of the *detected* Cl fragments stems

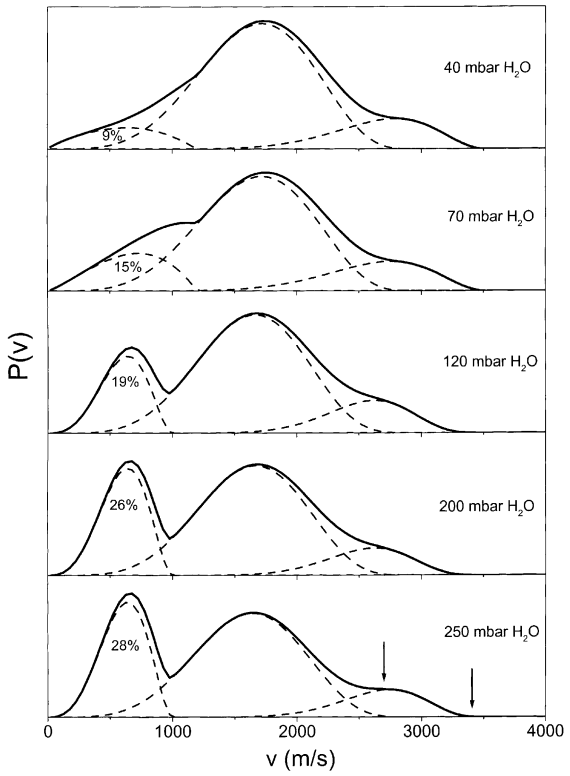

Fig. 4. $Cl(^2P_{3/2})$ photofragment speed distributions $P(v)$ as a function of the partial water pressure $p(H_2O) = 40$–250 mbar. The expansion condition were 2 bar He with 0.4% $ClNO_2$. The arrows mark E_T^{max}.

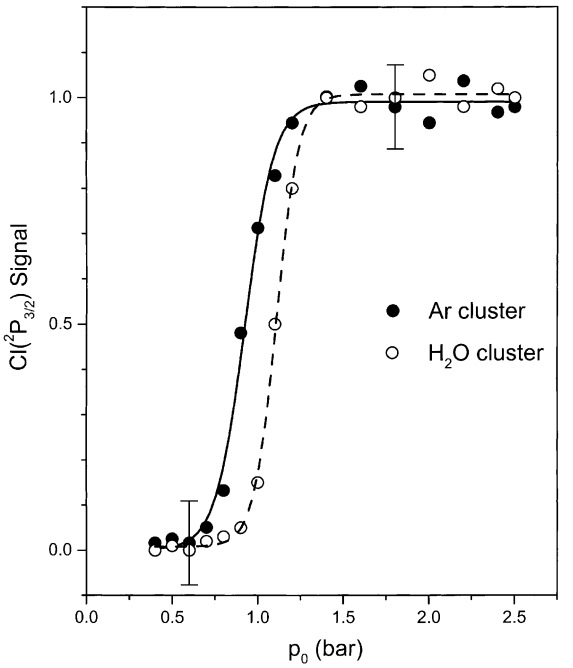

Fig. 5. Argon and water cluster formation as a function of the stagnation pressure p_0 measured for the slow component in Fig. 2. The expansion conditions were (a) 0.4% $ClNO_2$ with 200 mbar H_2O in helium and (b) 0.1% $ClNO_2$ in argon.

from free or at most very weakly cluster-bound $ClNO_2$.

The analysis of the slow Cl fragments from Fig. 2 shows an *isotropic* recoil and a Boltzmann velocity distribution with a temperature of 450 ± 100 K and 580 ± 100 K (corresponding to $\langle E_T \rangle$ of ~5.6 kJ/mol and ~7.2 kJ/mol) for the argon and water clusters, respectively. These findings allow us to assign the slow component to fragments which are initially generated by photolysis in the cluster interior. During the escape from the evaporating cluster cage they are thermalized and lose their vector correlation. The small $\langle E_T \rangle$ values calculated above (assuming $m_{Cl} < m_{Cluster}$) indicate that most of $E_{avl} = 370$ kJ/mol is transferred to the cluster cage. From inspection of Figs. 2–4 it appears as if the portion of the Cl cluster fragments would generally be small compared to all the Cl fragments. However in our cluster photodissociation we detect only the Cl fragments which escape the cluster cage and for the broad cluster size distribution created under our conditions we expect only small clusters to be melted upon photolysis. In large clusters the Cl fragments will remain caged.

Fig. 3 shows the relative portion of Cl cluster fragments to increase with decreasing $ClNO_2$ concentration (from 2% to 0.5%) i.e. a higher percentage of $ClNO_2$ molecules becomes incorporated in clusters. A similar effect is observed when the Ar pressure is increased. In the latter case this is ascribed to the decreasing expansion temperature with increasing stagnation pressure leading to more favorable cluster formation conditions. For water clusters (Fig. 4) the increase of the cluster material by increasing the H_2O partial pressure from 40 to 250 mbar produces more clusters and hence more Cl cluster fragments relative to those produced from the monomers.

Acknowledgements

Support by the Schweizerischer Nationalfonds and by the Alfred Werner Legat is gratefully acknowledged. We thank Rolf Pfister for the synthesis of $ClNO_2$ and PD Dr. P. Willmott for critically reading the manuscript.

References

[1] B.J. Finlayson-Pitts, M.J. Ezell, J.N. Pitts Jr., Nature 337 (1989) 241.
[2] M.A. Tolbert, M.J. Rossi, D.M. Golden, Science 240 (1988) 1018.
[3] M. Leu, J. Geophys. Res. Lett. 15 (1988) 851.
[4] D.J. Erickson III, C. Seuzaret, W.C. Keene, S.L. Gong, J. Geophys. Res. 104 (1999) 8347.
[5] W. C Keene, M.A.K. Khalil, D.J. Erickson III, A. McCulloch, T.E. Graedel, J.M. Lobert, M.L. Aucott, S.L. Gong, D.B. Harper, G. Kleiman, P. Midgley, R.M. Moore, C. Seuzaret, W.T. Sturges, C.M. Benkovitz, V. Koropalov, L.A. Barrie, Y.F. Li, J. Geophys. Res. 104 (1999) 8429.
[6] W. Behnke, C. George, V. Scheer, C. Zetzsch, J. Geophys. Res. 102 (1997) 3795.
[7] A.J. Illies, G.A. Takacs, J. Photochem. 6 (1976/77) 35.
[8] H.H. Nelson, H.S. Johnston, J. Phys. Chem. 85 (1981) 3891.
[9] A.J. Grimley, P.L. Houston, J. Chem. Phys. 72 (1980) 1471.
[10] F.E. Livingston, B.J. Finlayson-Pitts, Geophys. Res. Lett. 18 (1991) 17.
[11] B.J. Finlayson-Pitts, F.E. Livingston, H.N. Berko, Nature 343 (1990) 622.
[12] D.V. Michelangeli, M. Allen, Y.L. Yung, Geophys. Res. Lett. 18 (1991) 673.
[13] A. Furlan, M.A. Haeberli, J.R. Huber, J. Phys. Chem. A 104 (2000) 10392.
[14] JANAF Themochemical Tables, J. Phys. Chem. Ref. Data 14 (1985) suppl. 1.
[15] B. Kirmse, A. Delon, R. Jost, J. Chem. Phys. 108 (1998) 6638.
[16] J.L. Hardwick, J.C.D. Brand, Chem. Phys. Lett. 21 (1973) 458.
[17] A. Weaver, R.B. Metz, S.E. Bradforth, D.M. Neumark, J. Chem. Phys. 90 (1989) 2070.
[18] C.E. Miller, H.S. Johnston, J. Phys. Chem. 97 (1993) 9924.
[19] R.T. Carter, A. Hallou, J.R. Huber, Chem. Phys. Lett. 310 (1999) 166.
[20] J. Plenge, R. Flesch, M.C. Schürmann, E. Rühl, J. Phys. Chem. A 105 (2001) 4844.
[21] D. Salcedo, L.T. Molina, M.J. Molina, J. Phys. Chem. A 105 (2001) 1433.
[22] M.A. Zondlo, S.B. Barone, M.A. Tolbert, J. Phys. Chem. A 102 (1998) 5735.
[23] A.E. Waibel, Th. Peter, K.S. Carslaw, H. Oelhaf, G. Wetzel, P.J. Crutzen, U. Pöschl, A. Tsias, E. Reimer, H. Fischer, Science. 283 (1999) 2064.
[24] Q. Li, J.R. Huber, Chem. Phys. Lett. 345 (2001) 415.
[25] C.J. Kreher, R.T. Carter, J.R. Huber, J. Chem. Phys. 110 (1999) 3309.
[26] K. Bergmann, R.T. Carter, G.E. Hall, J.R. Huber, J. Chem. Phys. 109 (1998) 474.
[27] W.C. Wiley, I.H. Mclaren, Rev. Sci. Instrum. 26 (1955) 1150.
[28] C.E. Moore, Atomic Energy Levels, vol. 1, in: Circular 467, National Bureau of Standards, Washington, DC, 1949.
[29] M. Volpe, H.S. Johnston, J. Am. Chem. Soc. 78 (1956) 3903.
[30] U. Buck, R. Krohne, Phys. Rev. Lett. 73 (1994) 947.
[31] O.F. Hagena, Rev. Sci. Instrum. 63 (1992) 2374.